High-Efficiency, Microscale GaN Light-Emitting Diodes and Their Thermal Properties on Unusual Substrates

*Tae-il Kim, Yei Hwan Jung, Jizhou Song, Daegon Kim, Yuhang Li, Hoon-sik Kim, Il-Sun Song, Jonathan J. Wierer, Hsuan An Pao, Yonggang Huang, and John A. Rogers**

Materials and processing schemes for inorganic light-emitting diodes (LEDs) are increasingly important for applications in areas ranging from consumer electronics to energy-efficient lighting. Conventional routes to devices involve epitaxial growth of active materials followed by wafer dicing and pick-and-place robotic manipulation into individually packaged components, for interconnection by bulk wire bonding. Recently reported schemes based on advanced methods in epitaxial lift-off and deterministic assembly allow devices with extremely thin geometries, in layouts that can be interconnected by planar metallization and photolithography.[1–6]

Dr. T.-i. Kim, Y. H. Jung, Dr. D. Kim, Dr. H.-s. Kim, H. A. Pao, Prof. J. A. Rogers
Department of Materials Science and Engineering
Frederick Seitz Materials Research Laboratory
University of Illinois at Urbana-Champaign
Urbana, IL 61801, USA
E-mail: jrogers@uiuc.edu

Prof. J. Song
Department of Mechanical and Aerospace Engineering
University of Miami
FL 33146, USA

Y. Li, Prof. Y. Huang
Departments of Civil and Environmental Engineering and Mechanical Engineering
Northwestern University
Evanston, IL 60208, USA

Y. Li
School of Astronautics
Harbin Institute of Technology
Harbin 150001, China

I.-S. Song, Prof. J. A. Rogers
Department of Mechanical Science and Engineering
University of Illinois at Urbana-Champaign
Urbana, IL, 61801, USA

J. J. Wierer Jr.
Sandia National Laboratories
Albuguerque, NM, 87185, USA

Prof. J. A. Rogers
Departments of Chemistry and Electrical and Computer Engineering
Beckman Institute for Advanced Science and Technology
University of Illinois at Urbana-Champaign
Urbana, IL 61801, USA

DOI: 10.1002/smll.201200382

Alternative, related strategies involve LEDs comprising vertically aligned arrays of micro- or nanowires to offer similar advantages, including the ability to form devices on thin, plastic substrates,[7,8] but also with relaxed constraints on growth conditions. These and other recent advances have the potential to create new engineering opportunities and application possibilities for LED technologies. High-efficiency operation and facilitated thermal management through the use of arrays of microscale LEDs represent two key findings, of relevance for many envisioned applications.

This paper presents materials and fabrication strategies that enable efficient, ultrathin (slightly larger than 6 μm) LEDs based on GaN, with lateral dimensions ranging from ~1 mm × 1 mm to ~25 μm × 25 μm, and their integration onto unconventional substrates. The process begins with high quality epitaxial material grown using state-of-the-art techniques on sapphire substrates, but with unusual methods for releasing this material in the form of completed devices suitable for assembly using the techniques of transfer printing. This strategy represents a significant improvement over recently reported routes[1] to similar classes of devices, which rely critically on comparatively low-performance active materials grown on silicon. Particular additional points of emphasis in the following are theoretical and experimental aspects of heat dissipation with devices mounted on hydrogels and other 'soft' substrate materials, as models for their integration with organs of the body.

Figure 1 outlines the growth and processing steps, in a sequence of schematic illustrations, microscopy images and pictures. Figure 1A shows commercially obtained epitaxial material on sapphire, etched into square islands (100 μm × 100 μm) with L-shaped current-spreading layers (Ni: 15 nm/ Au 15 nm) and pads in the corners for top p-contacts (upper right; 25 μm × 25 μm; Cr: 15 nm/Au: 300 nm), and recessed n-contacts (lower left; 25 μm × 25 μm; Cr: 15 nm/Au: 300 nm). Details appear in the Experimental Section and in Figure S1 in the Supporting Information (SI). Uniform deposition of a thin layer (200 nm) of SiN_x passivates and protects the top surfaces and sidewalls of these structures, as preparation for coating with a bilayer of Cr (adhesion layer: 15 nm)/ Pd (150 nm) that facilitates bonding to another substrate (silicon or glass) which supports metallization of Cr (adhesion layer: 15 nm)/ Pd (150 nm)/ In (900 nm). Bonding at pressures and temperatures of 400 bar and 220 °C, respectively,

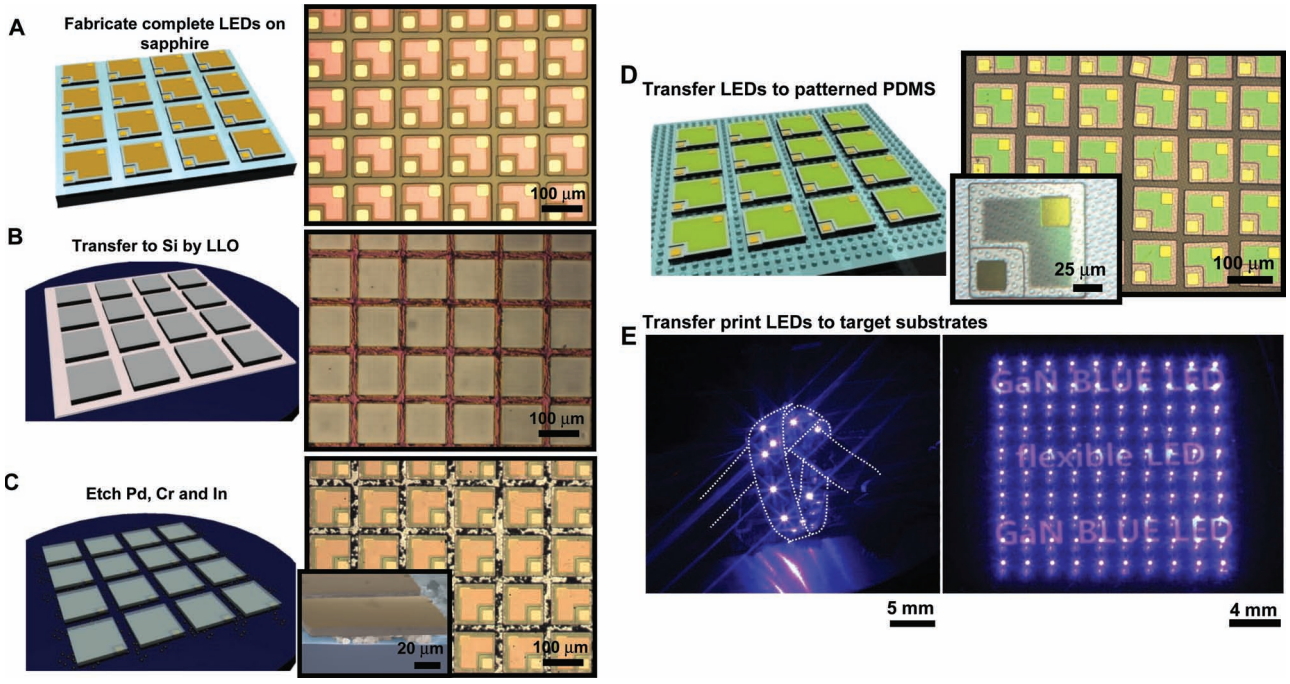

Figure 1. Schematic illustrations and images corresponding to steps for forming, integrating, and interconnecting ultrathin (~6 μm), microscale inorganic light-emitting diodes (μ-ILEDs) derived from GaN materials grown epitaxially on sapphire substrates. A) Arrays of μ-ILEDs (100 μm × 100 μm separated by 20 μm; left: schematic; right: optical microscopy image) are first defined, completely, on the sapphire substrate, including L-shaped current-spreading p-contacts (Ni:15 nm/Au:15 nm) and square (25 μm × 25 μm) n- and p- contact pads (Cr: 15 nm/Au:300 nm). B) Bonding to a silicon wafer using an In-Pd alloy, followed by laser lift-off and removal of the sapphire substrate yields arrays of μ-ILEDs on Si (dark blue). The top sides of the devices (left: schematic; right: optical microscopy image), coated with Ga (gray) from the LLO process, can be cleaned by etching with HCl. This etchant also removes unalloyed In, to leave only In-Pd alloy. C) Schematic illustration (left), optical microscopy image (right) and colorized, tilted view scanning electron microscopy (SEM) image (right inset) after these etching processes. Only isolated agglomerates of In-Pd (black dots in the optical microscopy image and schematic; pink structures in the SEM) remain. D) Arrays of μ-ILEDs after transfer to the structured surface of a slab of PDMS (arrays of pillars diameters, heights and spacings of 3, 1.4, and 5 μm, respectively) and complete removal of residual metal by etchants for Cr and Pd (left: schematic; right: optical microscopy image). A layer of SiN_x protects the μ-ILED metallization from these etchants. The inset on the right shows an individual device. E) Arrays of μ-ILEDs (12 devices) on a 4 mm × 15 mm strip of PET, tied into a knot to illustrate its deformability (left) and on glass (100 devices; right).

causes the In (melting point ~156 °C; Brinell hardness 8.83 MPa (cf. lead (Pb): 38.3 MPa))[9] to flow and partially fill the recessed n-contacts and the trenches between the devices. A fraction of the In alloys with the Pd,[10,11] to form a solid layer ($InPd_x$) that prevents cracking in the LEDs during subsequent processing, including laser lift-off (LLO) as described next.

Passing light from a krypton fluoride (KrF) (0.9 J/cm^2, 248 nm wavelength) or yttrium aluminum garnet (YAG): Nd laser (0.3 J/cm^2, 266 nm, single pulse with 5 ns exposure time) through the sapphire leads to strong absorption at the interface with the GaN, where thermal decomposition forms Ga metal and nitrogen gas. Pressure associated with this process releases the GaN from the sapphire, in the form of individual microscale inorganic LEDs (μ-ILEDs). Heating to 70 °C (melting point of Ga is 29.7 °C[9]) and applying mild mechanical force enables complete removal of the sapphire, as in Figure 1B and Figure S2 (SI). Immersing the exposed μ-ILEDs in dilute HCl (5 wt%) etches away the residual Ga, to yield clean surfaces on top. This same etchant removes unalloyed In, leaving only agglomerates of $InPd_x$. This remaining metal is important because it tethers the μ-ILEDs to the underlying substrate, in their transferred locations. The microscopy image in Figure 1C shows a sample after these process steps. The tilted scanning electron microscope (SEM) image in the inset reveals voids and $InPd_x$ agglomerates between a representative μ-ILED and the substrate.

Contacting a bulk slab of poly(dimethylsiloxane) (PDMS) that has an array of vertical pillars (3 μm in diameter, 1.2 μm in height, and 5 μm spacings) embossed on its surface, and then peeling it away retrieves, in a single step, all of μ-ILEDs from their substrate via separation at the contact points defined by the $InPd_x$, leaving the devices bound by van der Waals forces to the structured surface of the PDMS. Etching the exposed Pd and Cr layers removes all residual metal particles (Figure S3 (SI) shows Si wafer after removal of all μ-ILEDs) including, by lift-off, any remaining particulates of $InPd_x$. Figure 1D presents optical microscopy images of the results; the inset shows an individual μ-ILED on a structured PDMS slab. (As shown in this image, a fraction of the devices, typically ~10%, undergo some translational and rotational misalignment during the transfer. This aspect of the process can be further minimized through optimized processing, or it can be accommodated in the steps described next.) Techniques

NANO MICRO small

of transfer printing are used to remove individual μ-ILEDs, or selected collections of them, from this PDMS slab and then to deliver them to nearly any substrate of interest, where they can be electrically interconnected to yield functional lighting systems using procedures described elsewhere (see Figure S4–6, SI).[1] For transparent substrates, the μ-ILEDs were electrically interconnected using photolithographic techniques after passivation by a "back-side exposure" method with a photocrosslinked planarization layer. For opaque substrates, such as Al foil, fully formed interconnected arrays were transferred, in whole, by transfer printing. The main focus of work presented here corresponds to systems in which the densely arrayed μ-ILEDs on the structured PDMS are distributed over large areas, in sparse coverages on soft substrates. Figure 1E (left) shows an interconnected string of 12 μ-ILEDs on a strip (5 mm × 40 mm) of poly(ethylene terephthalate) (PET, 50 μm thick; Grafix Dura-Lar film roll) and a square array of 100 μ-ILEDs on glass (right). Comparisons of performance in μ-ILEDs on sapphire and on PET (50 μm thick) (**Figure 2**A–D) reveal nearly identical behaviors at low power. At high power, the μ-ILEDs on sapphire show a slight blue-shift in emission wavelength (from 447 nm at 1 mA to 445.2 nm at 10 mA), consistent with charge accumulation that results from band filling effects described previously.[12,13] By contrast, μ-ILEDs on PET exhibit red-shift (from 447.3 nm at 1 mA to 451.7 nm at 10 mA) due to heating associated with the low thermal conductivity of the PET (compared to the sapphire).[13] (see Figure S7 and S8, SI) Although the measured operational characteristics do not reach levels of current, state-of-the-art devices, commercial materials show much improved performance, as illustrated in Figure S9 (SI).

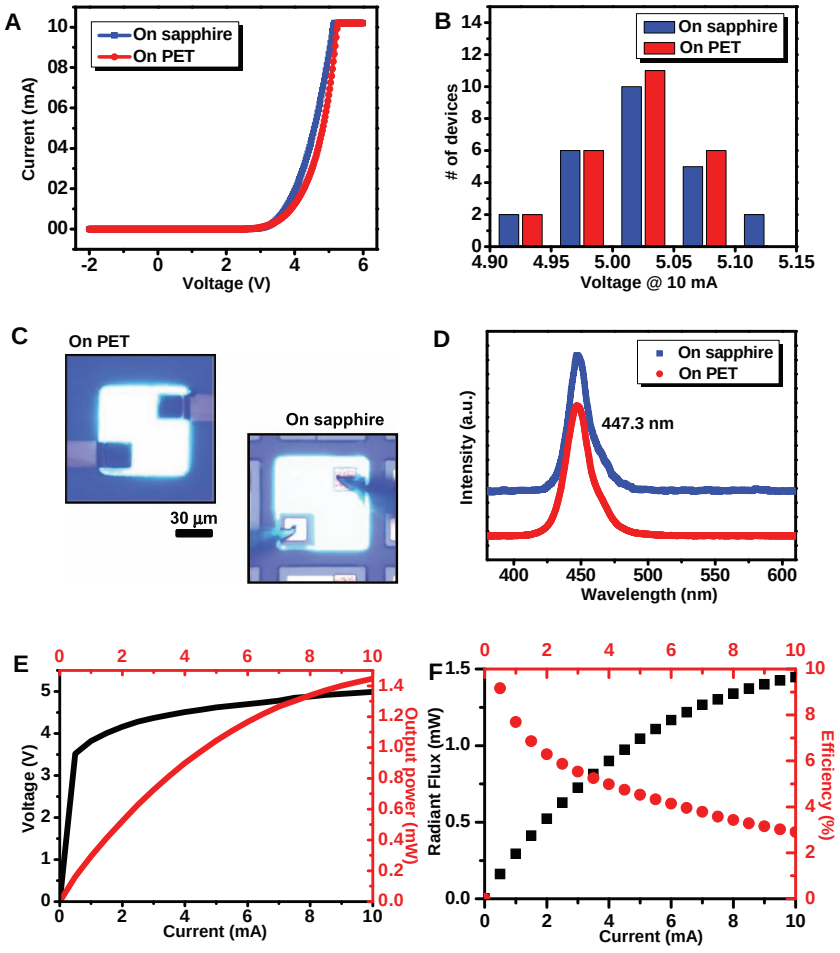

Figure 2. A,B) Electrical and C–F) optical properties of representative μ-ILEDs (100 μm × 100 μm) on a sapphire substrate, and on PET. A) Current–voltage (*I–V*) characteristics. B) Histogram of forward voltage at 10 mA current, measured on 25 μ-ILEDs on sapphire and on PET. C) Images of single μ-ILED on PET (left; at 3 mA) and sapphire (right; at 3 mA). D) Spectral properties of the emission from the devices shown in C. E) Light output-current and voltage (LIV) measurements for a μ-ILED on PET. F) Radiant flux and radiant efficiency (energy conversion efficiency) as functions of applied current, for a μ-ILED on PET.

As suggested by previous thermal modeling results, an advantage of μ-ILEDs is their accelerated rates of passive heat spreading due to favorable size scaling effects in thermal transport.[1] The strategy of Figure 1 is compatible with a wide range of μ-ILED sizes (much wider than previously possible[1]), in a manner that allows first quantitative experimental investigations of these effects. **Figure 3**A shows examples, from 1 mm × 1 mm, 500 μm × 500 μm, 300 μm × 300 μm, 150 μm × 150 μm, 100 μm × 100 μm, 75 μm × 75 μm, 50 μm × 50 μm to 25 μm × 25 μm^2. This size range spans the commercial regime to dimensions limited only by resolution and alignment accuracy of tools for photolithography used in this work. Even the largest devices show spatially uniform emission across the active regions (Figure 3B). Studies of size-dependent operational characteristics over this available range illustrate clearly the relevant behaviors. Figure 3C, for example, shows a sharp decrease in operating temperatures of μ-ILEDs on a 50 μm thick PET substrate, at the same power per unit area, with decreasing μ-ILED size. The results are significant reductions in the operating temperatures, and corresponding enhancements in efficiency (Figure 3C). These improvements can be illustrated in plots of the input and output power densities, shown in Figure 3D. The overlap of these data at low power densities suggests that the beneficial aspects of small device geometries (in the regime studied) are due mostly to thermal effects and not, for example, to increases in optical output coupling efficiency which might also occur. These output powers and junction temperatures for devices on PET show trends similar to those on sapphire.[12,13]

This improvement in thermal behavior with decreasing size can be exploited by structuring an LED with conventional dimensions into an array of interconnected μ-ILEDs with sufficient spacing, as suggested theoretically in our

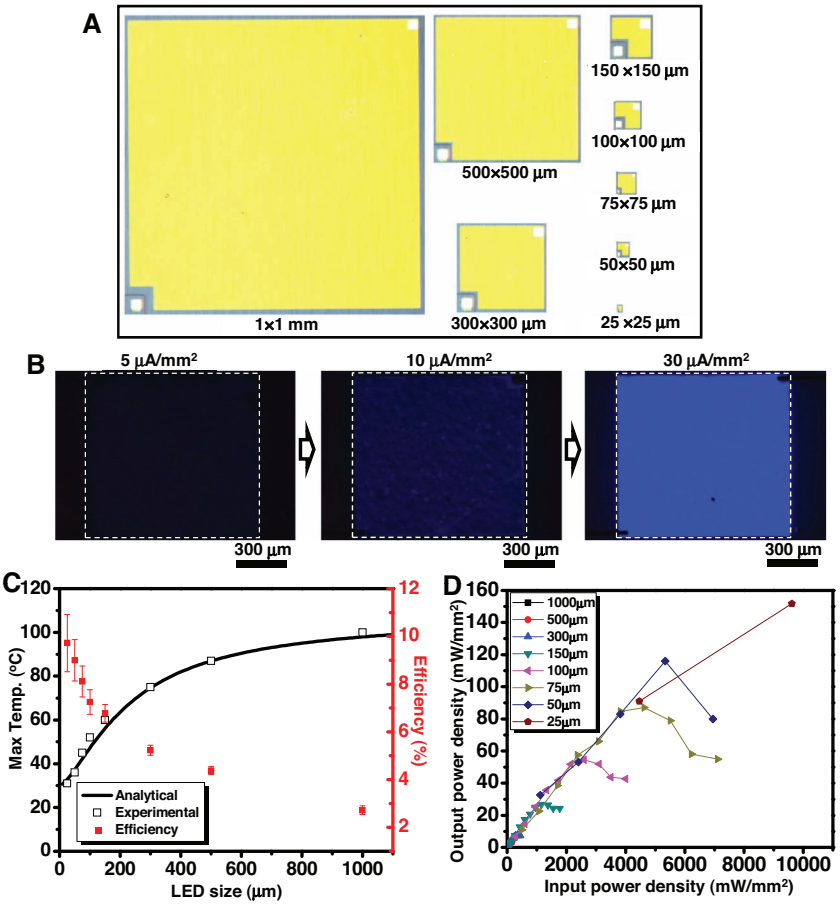

Figure 3. Size scaling effects in the operation of μ-ILEDs on a 50 μm thick PET substrate. A) Optical microscopy images of μ-ILEDs with lateral dimensions from 1 mm × 1 mm, 500 μm × 500 μm, 300 μm × 500 μm, 150 μm × 150 μm, 100 μm × 100 μm, 75 μm × 75 μm, 50 μm × 50 μm, to 25 μm × 25 μm. B) Microscopy images of emission from a representative 1 mm × 1 mm device, showing uniform output at three current densities: 5, 10, to 30 μA/mm^2. C) Measured (black symbols) and simulated (black line) maximum temperature as a function of μ-ILED size (lateral dimension), at 160 mW/mm^2 (For example, 40 mW at 500 μm × 500 μm μ-ILED and 160 mW at 1000 μm × 1000 μm μ-ILED). Red symbols show radiant efficiencies. D) Output (optical) power density as a function of input (electrical) power density, for μ-ILEDs with different sizes.

recent report.[1] **Figure 4** provides detailed experimental evidence of the effects. Here, two device designs are compared (Figure 4A). The first involves a single, 500 μm × 500 μm μ-ILED; the second is a 5 by 5 array of 100 μm × 100 μm μ-ILEDs, separated by 200 μm. Figure 4B and Figure S10 and S11 (SI) show heat dissipation results for the first case (red open circles, experimental; black lines, analytical models; black squares, finite element models) at 40 mW of applied power at room temperature. The peak device temperature is ~86 °C, with a characteristic lateral decay length of ~200 μm along the PET substrate (~50 μm thick). Separating adjacent μ-ILEDs in the 5 × 5 array by slightly more than 200 μm can yield significant reductions in peak temperatures. We performed measurements on arrays with various separations; the results for the peak temperatures appear in Figure 4C and Figure S12–S15 (SI), at applied powers of 20 and 40 mW. We note that the characteristic lateral decay length will be sensitive to many parameters, including the PET thickness, i.e., increasing the thickness increases this length. Some modeling results appear in Figure S10–S16 (SI). We also note that the electrical interconnects simultaneously provide heat sinking for these devices, due to their small size and small thermal mass.

As with the thickness, the intrinsic thermal properties of the substrate materials have a large effect on heat dissipation, consistent with expectation. **Figure 5** shows results from two dramatically different cases: 700 μm thick Al foil and 2 mm thick hydrogel. The μ-ILED on Al foil reaches only 48 °C at 40 mW of applied power (Figure 5A and Figure S17 (SI)) without degradation over several minutes of operation while an identical one on hydrogel reaches 65 °C even at only 5 mW (Figure 5B and Figure S18 (SI)). At 40 mW, this latter case leads to strong degradation of both the device and the substrate even with operation only for a few seconds, due to the high temperatures that are reached (cf. 232 °C at 30 mW). Nevertheless, as discussed above, small device geometries create opportunities for reliable operation even on such substrates, thereby suggesting their potential use on or under the skin or integrated with internal tissues of the body. Here, pulsed mode can provide additional benefits, especially in applications of optogenetics, where the biological response can be suppressed with continuous mode operation.[14] The thermal behaviors under pulsed operation are shown in Figure 5C for an μ-ILED on hydrogel, to simulate biological tissue, for various duty cycles (1, 10, 30, 50, 70, 90, and 100%) at 30 mW peak power. The various duty cycles of 1, 10, 30, 50, 70, 90, and 100% correspond to on and (off) times of 10 μs (990 μs), 100 μs (900 μs), 300 μs (700 μs), 500 μs (500 μs), 700 μs (300 μs), 900 μs (100 μs). As can be seen in simulation results in Figure 5C (open black circles, minimum tempearture; filled black circles, maximum temperature) and right images of D and Figure S19–S21 (SI), the time-dependent behavior of the temperature reflects the pulsed operational mode, with decreases in temperature between pulses, due to thermal diffusion. As the duty cycle decreases, so does the temperature, from 232 °C at 100% (Figure S19, SI) to 30.3 °C at 1% (Figure 5D and Figure S21 (SI)). For the regimes of operation explored here, reducing the duty cycle of the pulsed mode at short period (less than 1 ms) has similar effects to reducing the average power in a continuous (i.e., nonpulsed) mode (Figure S22 (SI)). For example, the temperature of a μ-ILED with 50% duty cycle and 1 ms period at 30 mW is about 128 °C (maximum and minimum of 154 and 102 °C, respectively), similar to the temperature (125 °C) at 15 mW continuous power. The characteristic times for passive cooling in this case are

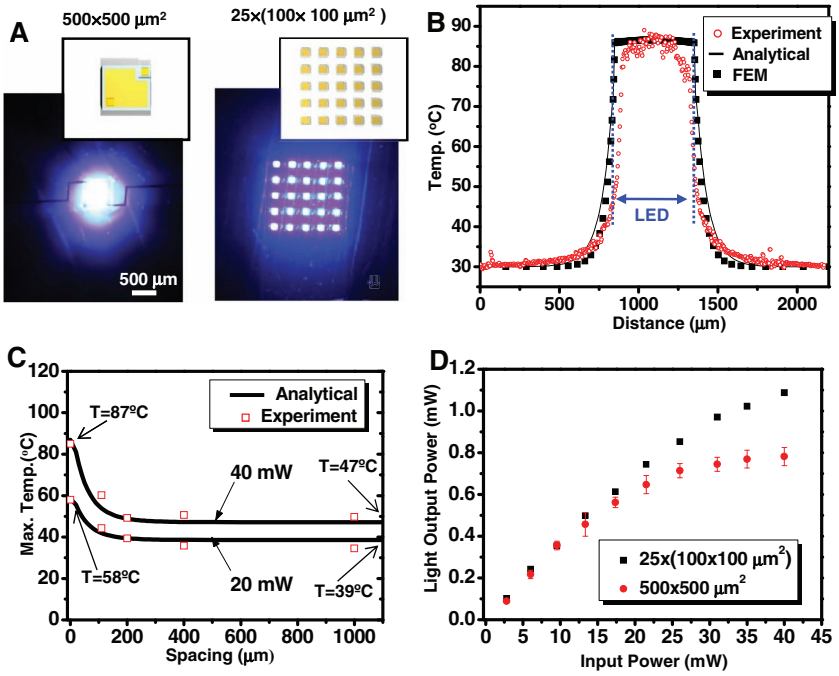

Figure 4. Thermal management by controlling size and spatial distributions of μ-ILEDs on PET. Optical images and emission profiles of a single device with size 500 μm × 500 μm and an equivalent active area consisting of a 5 × 5 array of devices with sizes of 100 μm × 100 μm. B) Measured (red open circles) and calculated (line, analytical model; black squares, FEM) distribution of temperature distribution along a dimension in the plane of a μ-ILED (500 μm × 500 μm) on PET, perpendicular to an edge and running through its center, for an applied power of 40 mW. C) Measured (red squares) and calculated (line, analytical model) maximum temperature of regular, square arrays (5 × 5) of μ-ILEDs (100 μm × 100 μm), with spacings of 0, 100, 200, 400, and 1000 μm. D) Total light output power as a function of electrical input power, for a single μ-ILED with size 500 μm × 500 μm and for a regular, square array of 100 μm × 100 μm μ-ILEDs (5 × 5), corresponding to the case shown in A.

~20 ms (Figure 5E). The pulsed mode shows promise for achieving challenging requirements in optogenetics, where peak powers must be ~10 mW/mm^2 with sustained changes in temperature of less than 1–2 °C.[14]

The results reported here suggest that state-of-the-art GaN epitaxial materials grown on sapphire substrates can be manipulated in the form of μ-ILEDs, for use in applications that would be difficult or impossible to address with conventional LED technologies. Applications in bio-integrated sensors and actuators appear particularly interesting. In these and other cases, use of epitaxial materials more advanced than those described here, together with modern output coupling schemes, can offer immediate further improvements in performance.

Experimental Section

Delineating μ-ILEDs and Formation of Ohmic Contacts: The fabrication began with GaN epitaxially grown on a double-sided polished sapphire wafer (2 inch diameter; Cermet Inc.) The epitaxial layers consisted of undoped GaN (3.8 μm), n-type doped GaN (2 μm), multiple quantum wells (0.14 μm), and p-type doped GaN (0.2 μm). Rinsing with diluted HCl (HCl:deionized (DI) water = 1:3) for 5 min removed residual metal ions and oxided GaN. Sputter deposition (AJA, ATC 2000) formed a bilayer of Ni (15 nm) and Au (15 nm) as a thin p-contact. Wet etching the Au (for 3 s) and Ni (for 2 min) with commercial etchants (Transene) patterned this bilayer into a L-shape for effective current spreading. The sample was annealed in an oxygen and nitrogen atmosphere at 500 °C for 5 min to enhance the contact properties. Next, patterning photoresist near the inner edges of the L-shaped pad and then removing the exposed epitaxial material by chlorine-based inductively coupled reactive ion etching (ICP-RIE; PlasmaTherm, SLR-770) formed square (40 μm × 40 μm) recessed regions to open access to the n-type layers at the base. In a single step, contact pads to the n- and p-regions, each 25 μm × 25 μm, were formed by electron beam evaporation (Temescal, FC-1800) of 15 nm of Cr and then 300 nm of Au. A low-stress silicon nitride (200 nm; SiN_x) was then formed uniformly over the entire substrate, using plasma enhanced chemical vapor deposition (PECVD; STS, Mesc Multiple). Next, a negative tone photoresist (PR, 7 μm thick; MicroChemicals Inc., AZ nLOF 2070) was patterned by photolithography, to serve as a mask for etching the SiN_x as well as the GaN to define the lateral dimensions of arrays of μ-ILEDs. As a final step, residual PR was removed by immersion in piranha solution (3:1 mixture of surfuric acid with hydrogen peroxide at 90 ºC) for 5 min.

Bonding and Laser Lift-Off (LLO): After delineating and forming contacts for the μ-ILEDs, another layer of SiN_x (200 nm) was deposited for passivation, as preparation for wafer bonding and transfer. The process used Cr (15 nm)/Pd (150 nm) on the SiN_x-coated μ-ILED substrate and Cr (15 nm)/Pd (150 nm)/In (900 nm) on a target silicon wafer. The bonding occured upon contact with a pressure of 400 bar and heating to 220 °C. The LLO used 0.9 J/cm^2 from a krypton fluoride (KrF) laser (JSPA, excimer laser with 248 nm wavelength) or 0.3 J/cm^2 from yttrium aluminum garnet (YAG) laser (Sandia Nat. Lab, third harmonic of a Q-switched YAG:Nd laser, 266 nm wavelength, single pulse with 5 ns exposure time), directed through the polished bottom surface of the sapphire. Absorption occurred at the GaN-sapphire interface, to cause decomposition of the undoped GaN into nitrogen (N_2) and gallium (Ga) metal according to:

$$2GaN \rightarrow 2Ga\,(m) + N_2(g)$$

The sample was then heated to 70 °C, to melt the Ga. Afterward, the sapphire substrate could be removed easily, to complete the transfer of GaN.

Transfer Printing of Individual μ-ILEDs: Immersion in dilute HCl (5% volume ratio) removed the unalloyed In in the vicinity of the bonding layer. The In-Pd alloy was not removed in this etchant, thereby leaving it to serve as distributed tethers (i.e., anchors) to hold the μ-ILEDs to the underlying silicon. Next, the residual Pd and Cr material on the passivated μ-ILEDs was eliminated by

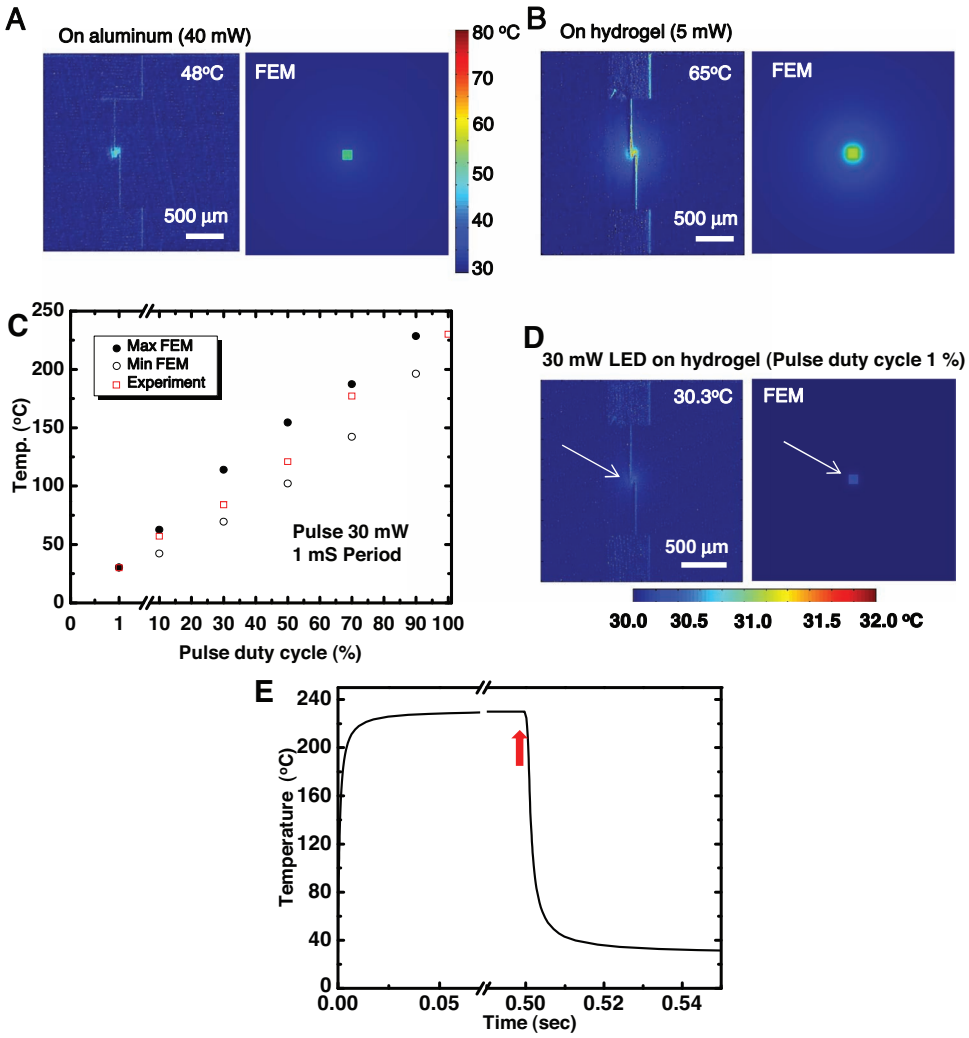

Figure 5. Thermal behavior of μ-ILEDs on unusual substrate materials. A) Measured (left) and calculated (right) temperature distributions for isolated μ-ILEDs (100 μm × 100 μm) on 700 μm thick Al foil at an input power of 40 mW. B) Results similar to those in (A), for the case of a hydrogel substrate and power of 5 mW. C) Temperature for a similar μ-ILED on hydrogel with 100 (constant power), 70, 50, 30, 10, and 1% duty ratio cycle pulse (30 mW input power with 1 mS period). D) The peak temperature decreases from 232 °C (at constant power) to 30.3 °C (at 1% pulsed duty cycle), as duty cycle decreases. E) Calculated time dependence of the peak temperature, near the switching point (red arrow).

Pd and Cr etchant (Transene Inc.), respectively. Contacting a bulk slab of PDMS with an array of vertical pillars (3 μm in diameter, 1.2 μm in height, and 5 μm in space) against the processed substrate and then quickly peeling it back transferred all of the μ-ILEDs to the structured surface of the PDMS. Etching the exposed Pd and Cr layers removed all residual metal. A PDMS stamp with posts (100 μm × 100 μm and heights of 100 μm) was positioned above the μ-ILEDs to allow their retreival and printing to a substrate of interest. The printing was performed using a slightly modified mask aligner (Karl Suss, MJB) or an automated printing machine. The structured PDMS slab is important because it allows the μ-ILEDs to be flipped over for further processing, in a way that provides sufficiently weak adhesion (defined by van der Waals interactions, and contact area) for efficient retreival by transfer printing.

Interconnected Arrays: To form interconnected arrays of μ-ILEDs, or for electricallly probing individual devcies, the SiN_x layer was first etched away by reactive ion etching (RIE; a mixture of CF_4 (40 sccm) and O_2 (1.2 sccm); Plasmatherm 790). Coating with an adhesion promoter (Dow, AP3000) and then a layer of photosensitive benzocyclobutene (6 μm thick; BCB) prepared the devices for backside exposure to ultraviolet light, through a transparent substrate. This light exposes the BCB in all regions except those above the opaque n-, and p- contact pads. Developing away the unexposed BCB (Advanced Developer, DS2100) and blowing with a stream of N_2 removed the residual developer, to complete the patterning process. After fully curing the BCB in Ar atomosphere glove box, remaining BCB residue was removed by oxygen RIE. To form metallization lines to the contacts, 15 nm of Cr and 300 nm of Au were sputtered, and then etched using a mask of patterned PR.

Characterization of Electrical, Optical, and Thermal Properties: A semiconductor parameter analyzer (4155C, Agilent) was used to measure the electrical properties. Optical measurements of the emission spectra and light output were performed with a spectrometer (HR4000 and FOIS-1 fiber optics integrating sphere, Ocean Optics). Radiant efficiency was simply calculated by P_{out}/P_{in}, where P_{out} and P_{in} are light output power and input (electrical) power, respectively. Thermal measurements were

performed using a MWIR-based InDb thermal imager (InfraScope, GFI) with a base temperature of 30 °C.

Supporting Information

Supporting Information is available from the Wiley Online Library of from the author.

Acknowledgements

Hydrogel sheets and commercial LEDs shown in Figure S9 (SI) are kindly provided by Dr. Cunjiang Yu and Cooledge Lighting Inc, respectively. Authors would like to thank Rak-Hwan Kim and Anthony Coley (Sandia Nat. Lab) for the assistance in photography and LLO, respectively. This material is based partly upon work supported by the Department of Energy, Division of Materials Sciences under Award No. DEFG02-91ER45439, through the Frederick Seitz MRL and Center for Microanalysis of Materials at the University of Illinois at Urbana-Champaign. For automatic printers, the authors acknowledge the center for Nanoscale Chemical Electrical Mechanical Manufacturing Systems in University of Illinois, which is funded by National Science Foundation under grant DMI-0328162. J.J.W. is supported by a multi-program laboratory managed and operated by Sandia Corporation, a wholly owned subsidiary of Lockheed Martin Corporation, for the US Department of Energy's National Nuclear Security Administration under contract DE-AC04-94AL85000.

[1] H.-S. Kim, E. Brueckner, J. Song, Y. Li, S. Kim, C. Lu, J. Sulkin, K. Choquette, Y. Huang, R. G. Nuzzo, J. A. Rogers, *Proc. Natl. Acad. Sci. USA* **2011**, *108*, 10072.

[2] S.-I. Park, Y. Xiong, R.-H. Kim, P. Elvikis, M. Meitle, D.-H. Kim, J. Wo, J. Yoon, C.-J. Yu, Z. Liu, Y. Huang, K.-c. Hwang, P. Ferreira, X. Li, K. Choqqette, J. A. Rogers, *Science,* **2009**, *325*, 977.

[3] X. Hu, P. Kull, B. d. Graff, K. Dowling, J. A. Rogers, W. J. Arora, *Adv. Mater.* **2011**, *23*, 2933.

[4] R.-H. Kim, M.-H. Bae, D. G. Kim, H. Cheng, B. H. Kim, D.-H. Kim, M. Li, J. Wu, F. Du, H.-s. Kim, S. Kim, D. Estrada, S. W. Hong, Y. Huang, E. Pop, J. A. Rogers, *Nano Lett.* **2011**, *11*. 3881.

[5] R.-H. Kim, D.-H. Kim, J. Xiao, B. H. Kim, S.-I. Park, B. Panilaitis, R. Ghaffari, J. Yao, M. Li, Z. Lui, V. Malyarchuk, D. G. Kim, A.-P. Le, R. G. Nuzzo, D. L. Kaplan, F. G. Omenetto, Y. Huang, Z. Kang, J. A. Rogers, *Nat. Mater.* **2010**, *9*, 929.

[6] K. J. Lee, J. Lee, H. Hwang, Z. J. Reitmeier, R. F. Davis, J. A. Rogers, R. G. Nuzzo, *Small* **2005**, *1*, 1164.

[7] K. Chung, C.-H. Lee, G.-C. Yi, *Science* **2010**, *330*, 655.

[8] C.-H. Lee, Y.-J. Kim, Y. J. Hong, S.-R. Jeon, S. Bae, B. H. Hong, G.-C. Yi, *Adv Mater.* **2011**, *23*, 4614.

[9] W. Assmus, S. Brühne, F. Charra, G. Chiarotti, C. Fisher, G. Fuchs, F. Goodwin, S. Gota-Goldman, S. Guruswamy, G. G. Gurzadyan, H. Harada, B. Holzapfel, K. U. Kainer, C. Kammer, W. Knabl, A.. Koethe, D. Krause, M. D. Lechner, G. Leichtfried, W. Martienssen, T. Mitsui, M. Müller, S. Pestov, G. Schlamp, B. Schüpp-Niewa, R. Stickler, P. Tzankov, V. Vill, H. Warlimont, in *Handbook of Condensed Matter and Materials Data* (Eds: W. Martinessen, H. Warlimont), Springer, Berlin, Germany **2005**, Part 2.

[10] Scientific group thermodata Europe (SGTE), P. Franke, D. Neuschutz, *Thermodynamics Properties, In-Pd (Indiun-Palladiun)*, Vol *19B5* (Eds: P. Franks, D. Neuschutz), Springer Materials, Berlin **2007**, Binary Systems part 5.

[11] a) W. S. Wong, Integration of GaN thin films with dissimilar substrate materials by wafer bonding and laser lift-off, Ph.D. thesis, University of California at Berkeley, USA., **1999**; b) W. S. Wong, T. Sands, N. W. Cheung, M. Kneissl, D. P. Bour, P. Mei, L. T. Romano, N. W. Johnson, *Appl. Phys. Lett.* **2000**, *77*, 2822.

[12] B.-J. Pong, C.-H. Chen, S.-H. Yen, J.-F. Hsu, C.-J. Tun, Y.-K. Kuo, C.-H. Kuo, G.-C. Chi, *Solid State Electron.* **2006**, *50*, 1588.

[13] Z. Gong, S. Jin, Y. Chen, J. Mckendry, D. Massoubre, I. M. Watson, E. Gu, M. D. Dawson, *J. Appl. Phys.* **2010**, *107*, 013103.

[14] M. E. Llewellyn, K. R. Thompson, K. Deisseroth, S. L. Delp, *Nat. Med.* **2010**, *16*, 1161.

Received: January 11, 2012
Published online: April 2, 2012